Spatially periodic patterns in a dc gas-discharge system

C. Radehaus,* H. Willebrand, R. Dohmen, and F.-J. Niedernostheide
Institut für Angewandte Physik, Universität Münster, 4400 Münster, Federal Republic of Germany

G. Bengel
Mathematisches Institut, Universität Münster, 4400 Münster, Federal Republic of Germany

H.-G. Purwins
Institut für Angewandte Physik, Universität, Münster, 4400 Münster, Federal Republic of Germany
(Received 23 May 1991)

The evolution of spatially periodic patterns lateral to the current flow in a dc gas-discharge system consisting of a semiconductor and a metal electrode is reported. To explain these experiments a previously introduced two-layer model is used, which can be described by a system of reaction-diffusion equations. The discretized form of this system of equations can be interpreted as an equivalent electric circuit. Applying the center manifold theory to the system of equations, the experiments can be explained in terms of a bifurcation in that the system is undergoing a Turing diffusion instability. For the model, as well as in the experiments, the bifurcation from a homogeneous state into a spatially periodic structure is obtained by varying the externally applied voltage, the load resistance, or the width of the discharge slit. In connection with the application of the model to the gas-discharge system, the $j(U)$ characteristic is measured for the whole discharge space and the positive column.

PACS number(s): 52.80.−s, 05.60.+w

I. INTRODUCTION

In nature the formation of time-spatial patterns in open thermodynamic systems driven far from equilibrium and dissipating energy is a well-known phenomenon and has attracted much interest in the past decade. Some well-known examples in chemistry, physics, and biology are the Belousov-Zhabotinskii reaction [1], laser [2], Rayleigh-Bénard convection [3], as well as the morphogenetic models of Gierer and Meinhardt [4]. Theoretical investigations concerning more general aspects of these phenomena were carried out, e.g., in Refs. [5–8].

By using an electric field as driving force we find a wide class of physical systems or materials which show interesting phenomena such as self-generated oscillations, stable pattern formation, or chaotic behavior due to the electric current flow. In recent time interesting work has been done on pattern formation in semiconductor materials. Examples are the studies of electric-field domains [9] and the dual case of filamentation of the electric current density in semiconductor devices [9–17]. The phenomenon of pattern formation has also been observed in gas-discharge devices. There are several investigations concerned with structures along the axis of the current flow [18,19]; we especially want to mention the well-known phenomenon of standing or moving striations [20,21]. Besides this, there are also examples for pattern formation transversal to the current flow, e.g., the two-dimensional complex rf discharge of Boyers and Tiller [22,23], the resistive electrode-discharge gap structure of Astrov and Portsel [24], and the formation of anode spots in a dc discharge system of Müller [25]. The pattern formation transversal to the current flow in a certain dc driven gas-discharge system was discussed in a previous work [26]. In this quasi-one-dimensional arrangement one of the electrodes consists of copper and the other of N-type doped silicon. The discharge slit is covered by glass plates. This type of device is the prototype of systems which can be described by the two-layer model proposed in Ref. [27] and was established for a certain situation in more detail in Ref. [28]. The equations describing the model lead to a two-component reaction-diffusion system. One of the components is a current density, the other component is given by an electric potential. In a certain range of operation the two components behave like activator and inhibitor in the morphogenetic models of biomathematics [4] and realize the essential features for stable spatial pattern formation. The model applies to a class of devices which is characterized by the property that the $j(E)$ characteristic is not constant in the direction of the current flow, but can be separated into a layer with a negative differential conductivity and a layer with Ohmic behavior (positive differential conductivity) according to the two layers of the model. Examples for applications of this model are semiconductor materials [27,29], especially p-i-n diodes [11,12] and the above-mentioned gas-discharge system.

In this paper we describe the experimental setup of the gas-discharge system and the application of the model to this system. For this purpose we determine the local $j(U)$ characteristic for different spatial regions of the whole discharge space to identify the nonlinear layer. We investigate experimentally the bifurcation from a stable homogeneous high current state into a spatially periodic distribution of the light density in the gas-discharge slit. These patterns are predicted by the model with bifurcation analysis.

The outline of the paper is as follows. In Sec. II we call to mind the two-layer model and present results from bifurcation analysis concerning the formation of spatially periodic structures. In Sec. III the experimental setup of the gas-discharge system and the experimental results are described. in Sec. IV the measured $j(U)$ characteristics for the whole discharge space and for the positive column are presented, and the layers of the model are identified. Furthermore, the experimental results are compared to the predictions of the model. In Sec. V some final conclusions are drawn.

II. TWO-LAYER MODEL AND SOME ANALYTICAL RESULTS

A. Model

The physical model of Ref. [27], which is shown in Fig. 1, consists of two layers, one of which has linear Ohmic electric properties, while the other has a nonlinear characteristic which contains a region of negative differential resistivity. The thickness a of the nonlinear layer is assumed to be very small compared to the thickness b of the linear layer. Applying an external voltage to the contacts by the load resistance R_S, the mean current flow direction will be the z direction. The behavior of the physical system can be described in terms of the distributions of a current density component and the electric potential at the interface Ω. Starting from the Poisson equation, the continuity equations, and the transport equations for positive and negative charge carriers with fixed diffusion and mobility coefficients, deviations of the charge carriers from a reference state, which is homogeneous in the x direction, are considered. With the assumption that the deviations behave quasineutrally, one equation is obtained for the density deviation n_1 of both the positive and negative charge carriers. At the reference state the charge-carrier density and the velocity of the charge carriers are given by (n_0, v_0). (Quantities labeled by "0" refer to the reference state.) Deviations from the reference state can be described by (n_0+n_1, v_0+v_1) with the corresponding current density $j_{\rm tot}=(n_0+n_1)(v_0+v_1)$. The partial differential equation for n_1 can be transformed into an equation for the current density $j=j(x,y,z,t)=j_0+n_1v_0$, which, however, allows for the determination of $j_{\rm tot}$ (cf. Ref. [28]). Averaging the partial differential equation for $j(x,y,z,t)$ with respect to z, we obtain an equation for the averaged current density $j=j(x,y,t)$ dependent upon the potential $U(x,y,t)$ in the interface layer Ω. This equation is similar to the usual transport equation with an "effective reaction term" F. Owing to the averaging procedure this term can be identified with the experimentally determined current-voltage characteristic of the nonlinear medium in the case of homogeneously distributed current density as outlined in detail in Ref. [28]. Choosing a suitable ansatz for the potential distribution in the linear layer [27], one can derive a two-component reaction-diffusion equation for the deviations j and U of the current density and the electrical potential in the interface. This is carried out in Ref. [28] for the two cases $\epsilon_N/a \ll \epsilon_L/b$ and $\epsilon_N/a \gg \epsilon_L/b$, where ϵ_N and ϵ_L are the dielectric constants of the nonlinear and linear layers, respectively. From numerical simulations we know that the latter case favors homogeneous oscillations, which were never observed in the gas-discharge system under discussion. In this work we therefore refer to the first case, which matches the properties of the gas-discharge system better. Furthermore, due to $l \gg d$, we can restrict our considerations to the quasi-one-dimensional case. If the potential U remains in a small vicinity of U_0, and if j_0/U_0 is small, the model can be described by the equations [28]

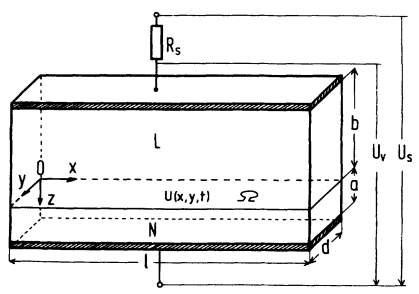

FIG. 1. The physical two-layer model consisting of a resistivity layer denoted by L and a nonlinar layer denoted by N; the hatched areas are metal electrodes.

$$\frac{\partial V}{\partial \tau}=\sigma\Delta V+\mu(\nabla V)(\nabla W)+F(V,A)-W+\chi-\frac{r}{L}\int_0^L V(\xi')d\xi' , \tag{1a}$$

$$\delta\frac{\partial W}{\partial \tau}-\delta\frac{\partial(\Delta W)}{\partial \tau}=\Delta W+V-W , \tag{1b}$$

with Neumann boundary conditions.

The dimensionless variables V and W correspond to the deviations from the current density j_0 and from the potential difference $U_{L0}=U_{V0}-U_0$, respectively (cf. Fig. 1). The normalized quantities and parameters are given by

$$V=(j-j_0)/j^*, W=(U_L-U_{L0})/U_L^*, \quad U_L^*/j^*=b\rho , \quad \xi=x/d_W^{1/2}, \quad \tau=(b\rho/\ell)t \tag{1c}$$

and

$$d_V=D_0\ell/(\rho b), \quad d_W=\tfrac{5}{26}b^2, \quad \sigma=d_V/d_W=26D_0\ell/(5\rho b^3),$$
$$\mu=26\mu_0 j^*\ell/(5b^2), \quad \delta=\epsilon_0\epsilon_L\rho^2 b/\ell ,$$
$$F(V,A)=-h(j^*V,A)/U_L^* ,$$
$$\chi=[U_0-H(j_0,A)]/U_L^*+\kappa-\kappa_0+(r-r_0)\nu_r , \tag{1d}$$
$$\kappa=U_S/U_L^*, \quad r=R_S l/\rho b, \quad \nu_r=\rho b j_0/U_L^* ,$$
$$L=l/(d_W)^{1/2}, \quad A=a/(d_W)^{1/2} ,$$
$$\nabla=\partial/\partial\xi, \quad \Delta=\partial^2/\partial\xi^2 .$$

One of the quantities U_L^* and j^* can be chosen arbitrarily. The meaning of the parameters is as follows. ℓ is a distributed inductance, D_0 and μ_0 are the ambipolar

diffusion constant and the mobility, respectively, ρ is the specific resistivity of the linear layer, and l, a, and b are geometrical quantities according to Fig. 1. As an extension of the system of equations of Ref. [28] we take into account variations of the parameters r and A corresponding to the load resistance R_S and the width a of the nonlinear layer, respectively. This leads to additional terms in the parameter χ compared with Ref. [28].

The functions h and H arise from a splitting of the $j(U)$ characteristic where j is the current density mentioned above. This $j(U)$ characteristic can be derived from measurements of the total $j_{\text{tot}}(U)$ characteristic as described in Ref. [28]. In this way the typical features of the nonlinear medium can be taken into account using experimentally accessible quantities without knowing the underlying microscopic processes. The variable j of Eqs. (1c) is given by

$$j(U)=j_0+n_1 v_0=j_0+\frac{s_2 U_0}{A}n_1(U) ,$$

where s_2 is a proportionality factor and n_1 is the deviation of the charge-carrier density for the positive as well as for the negative charge carriers from its corresponding value n_0 in the reference state. Variations of U are followed by variations of n_1 and j. Solving to U we obtain a system of curves $U=H(j,A)$. Choosing a reference state $U_0=H(j_0,A_0)$ we can split the characteristic $H(j,A)$ according to

$$H(j,A)=H(j_0,A)+h(j-j_0,A) .$$

In the reference point we have $h(0,A_0)=0$, i.e., $F(0,A_0)=0$, and $\chi=0$. By a linear expansion of the terms $U_0-H(j_0,A)$ in the deviations $A-A_0$ we obtain for χ

$$\chi=-(A-A_0)\nu_A+\chi-\chi_0+(r-r_0)\nu_r ,$$

with $\nu_A=[\partial H(j_0,A_0)/\partial A]/U_L^*$. This expression for χ is used in the following.

B. The equivalent circuit

In the case $\mu=0$ the discretized form of system (1) with a discretization according to Euler can be interpreted as equivalent electric circuit, which is shown in Fig. 2. This is an extension of the electric network, which was investigated in Refs. [30–35].

The equivalent circuit is a periodic chain of elements, each of which represents the spatially uncoupled behavior of the system of equations above. The nonlinear layer is presented by a nonlinear resistance and an inductance, which describes the time behavior of the nonlinear material modeling the generation and recombination processes of charge carriers. The nonlinear resistance is realized by a special electric circuit, which is described in detail in Ref. [33]. Internal points of these circuits are connected by a linear resistivity network of resistances R_i, which simulates the diffusion of the current density. The linear layer is formed by the resistance R_U. By means of the resistances R_V the potential of each cell is influenced by the potential of the adjacent cells. This portrays the potential diffusion of Eq. (1b). As the main capacity is located in the linear layer, each resistance current is coupled with a dielectric displacement current. So we approximate the properties of the linear material by capacitors parallel to R_U as well as to R_V. By applying Kirchoff's rules we can obtain a system of equations in terms of the voltages U_L^k across the resistance R_V and the current I^k through the inductance of the kth nonlinear element. These equations represent the spatially discretized form of Eqs. (1).

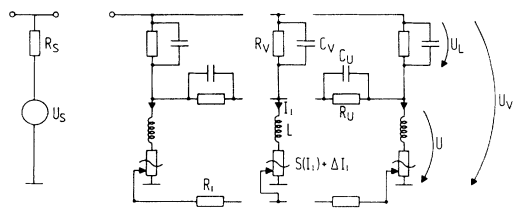

FIG. 2. Equivalent circuit representing the spatially discretized form of Eqs. (1) except for the drift term.

C. Bifurcation analysis

The system of equations (1) shows a rich repertoire of static and dynamic behavior, especially the formation of stable spatially inhomogeneous patterns. Numerical results for the case $r=r_0$ and $A=A_0$ are given in detail in Ref. [28]. In the following we show that the behavior of the system in the vicinity of a Turing [36] bifurcation point can be described by an equation of the Ginzburg-Landau-type.

For given parameters system (1) has a spatially homogeneous stationary state V_S, W_S given by the equations

$$\begin{aligned} &F(V_S,A)-W_S+\chi-rV_S=0 ,\\ &V_S-W_S=0 . \end{aligned} \tag{2}$$

Introducing the translated variables $v=V-V_S$ and $w=W-W_S$, this stationary state is transformed to $v=0, w=0$ and the system (1) now becomes

$$\begin{aligned} &\frac{\partial v}{\partial \tau}=\sigma\Delta v+\mu(\nabla v)(\nabla w)+f(v)-w-\frac{r}{L}\int_0^L v\,d\xi ,\\ &\delta\frac{\partial w}{\partial \tau}-\delta\frac{\partial(\Delta w)}{\partial \tau}=\Delta w+v-w , \end{aligned} \tag{3a}$$

where $f(v)=f(v;A,r,\kappa)=F(v+V_S)-F(V_S)$ with $V_S=V_S(A,r,\kappa)$, so $f(0)=0$. In addition we have the Neumann boundary conditions $(\nabla v)(0)=(\nabla v)(L)=(\nabla w)(0)=(\nabla w)(L)=0$.

In order to have a system of evolution equations we apply the inverse G of the operator $Id-\Delta$, i.e., Green's function of the boundary value problem $w-\Delta w=0$, $(\nabla w)(0)=(\nabla w)(L)=0$ to the second equation of (3a) and get

$$\begin{aligned} &\frac{\partial v}{\partial \tau}=\sigma\Delta v+\mu(\nabla v)(\nabla w)+f(v)-w-\frac{r}{L}\int_0^L v\,d\xi ,\\ &\delta\frac{\partial w}{\partial \tau}=Gv-w . \end{aligned} \tag{3b}$$

Linear stability analysis now tells us that the stationary solution $U'=(v,w)=(0,0)$ is stable, if the eigenvalues of the linear part of Eq. (3b) have a negative real part and a bifurcation occurs, if by changing the parameters of the problem one of the eigenvalues crosses the imaginary axis. To calculate these eigenvalues we develop v and w with respect to the orthonormal eigenfunctions $\varphi_n(\xi)$ of the Laplace operator with Neumann boundary conditions. In the one-dimensional case considered here the eigenvalues are $-k_n^2$, where $k_n=n\pi/L$, $n=0,1,\ldots,$ and the corresponding eigenfunctions φ_n are

$$\varphi_n(\xi)=(2/L)\cos(k_n\xi) \quad \text{for } k_n\neq 0,\ \varphi_0=1/L\ .$$

In this orthonormal basis Eqs. (3b) can be written as an infinite system of ordinary differential equations

$$\frac{\partial U_n'}{\partial\tau}=C_n' U_n'+N_n'(U')\ , \tag{4}$$

where

$$C_n'=\begin{bmatrix} a_n' & b_n \\ c_n & d_n \end{bmatrix},$$

$$U'=\sum_{n=0}^{\infty} U_n'(\tau)\varphi_n(\xi)\ ,$$

$$N_n'=\begin{bmatrix} \langle \varphi_n | N_V' \rangle \\ 0 \end{bmatrix},$$

with $a_n'=-\sigma k_n^2+f'-\delta_{0n}r$, $b_n=-1$, $c_n=[\delta(1+k_n^2)]^{-1}$, $d_n=-1/\delta$,

$$f'=\left[\frac{\partial f}{\partial v}\right](0),\quad N_v'=\sum_{i=2}^{\infty}\frac{1}{i!}\frac{\partial^i f}{\partial v^i}\bigg|_0 v^i+\mu(\nabla v)(\nabla w)\ ;$$

$\langle\ |\ \rangle$ denotes the usual scalar product.

We denote the eigenvalues of C_n' by $\omega_{\pm}(k_n)$ given by the equation

$$\omega(k_n)^2-\omega(k_n)\mathrm{Tr}(C_n')+\mathrm{Det}(C_n')=0\ .$$

If $\mathrm{Re}[\omega_{\pm}(k_n)]$ is negative for all k_n, the system is linearly stable. This is fulfilled if $\mathrm{Det}(C_n')>0$ and $\mathrm{Tr}(C_n')<0$ for all n.

There are two ways, in which the system may become linearly unstable depending on the behavior of the eigenvalues $\omega(k_n)$. In the first case, called hard-mode instability, two complex eigenvalues cross the imaginary axis. In the second case, called soft-mode instability, one real eigenvalue crosses the imaginary axis, while the real parts of the other eigenvalues remain less than zero. These two cases are given by $\mathrm{Tr}(C_n')=0$ and $\mathrm{Det}(C_n')=0$, respectively. Solving these conditions with respect to f' we get two neutral curves $f_H'(k)$ and $f_S'(k)$ for the hard-mode and soft-mode instabilities, respectively (see Fig. 3), which are defined at the discrete points $k_n=n\pi/L$, $n=0,1,\ldots,$:

$$f_H'(k)=\begin{cases}\sigma k^2+1/\delta & \text{for } k>0\\ 1/\delta+r & \text{for } k=0\ ,\end{cases} \tag{5a}$$

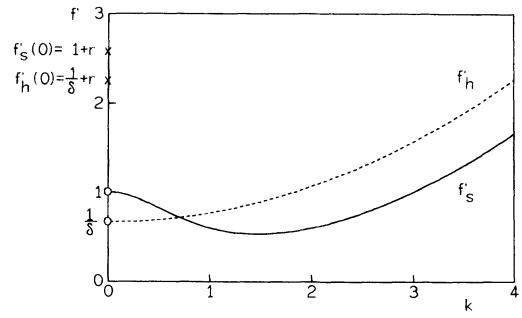

FIG. 3. Typical neutral curves for the hard-mode and soft-mode instability of system (2) in the case $\sigma<1$. Parameters: $\sigma=0.1$, $r=1.6$, $\delta=1.5$.

$$f_S'(k)=\begin{cases}\sigma k^2+1/(1+k^2) & \text{for } k>0\\ 1+r & \text{for } k=0\ .\end{cases} \tag{5b}$$

We now assume that one mode $k_c\neq 0$ becomes unstable in that the eigenvalue $\omega_+(k_c,f')$ becomes zero in dependence of the slope f' and crosses the critical point with positive velocity for growing f'. The critical eigenvalue $\omega_+(k_c f')$ is denoted by $\lambda=\lambda(f')=\lambda(f_c'+\Delta f')$; $\Delta f'$ serves as bifurcation parameter with $\lambda(f')=\lambda(f_c')=0$ for $\Delta f'=0$. The critical value k_c is approximately the local minimum of the function $f_S'(k)$, which is given by

$$k_c=(\sigma^{-1/2}-1)^{1/2}\ . \tag{6a}$$

The corresponding value of f_c' at this minimum is

$$f_c'=f_S'(k_c)=2\sigma^{1/2}-\sigma. \tag{6b}$$

A supposition for the occurrence of a soft-mode instability is that the minimum of f_S' is less than the minimum of f_H'. This assumption represents the scenario of the diffusion driven Turing instability. To describe the behavior near the instability point we follow the center manifold approach according to Ref. [37].

To get the appropriate system for the center manifold approach we consider $\Delta f'$ as an additional variable. The following system of equations:

$$\frac{\partial U_n'}{\partial\tau}=C_n U_n'+N_n\ ,$$

$$\frac{\partial(\Delta f')}{\partial\tau}=0\ ,$$

with

$$C_n=\begin{bmatrix} a_n & b_n \\ c_n & d_n \end{bmatrix}=C_n'(f'=f_c'),\quad N_n=N_n'+\begin{bmatrix}(\Delta f')v\\ 0\end{bmatrix},$$

is obtained. This is an infinite-dimensional ordinary system of equations, which can be rewritten as

$$\frac{\partial U}{\partial\tau}=CU+N(U) \tag{7}$$

by denoting $U=(v_0,w_0,\ldots,v_n,w_n,\ldots;\Delta f')^T$. This system has two eigenvalues zero with the corresponding eigenvectors

$$e_1 = m\,(0,0,\ldots,0,0,1,-a_c/b_c,0,0,\ldots,0,0;0)^T\,,$$
$$e_2 = (0,0,\ldots,0,0;1)^T\,, \tag{8}$$

where $m = (1+a_c^2/b_c^2)^{-1/2}$.

According to the center manifold approach the variable U is split into a linearly stable part U_S and a linearly unstable mode $U_U = pe_1 + (\Delta f')e_2$ with p as the amplitude of the unstable mode e_1

$$U = PU + P_S U = U_U + U_S$$

by means of the projection operators

$$P = P_1 + P_2$$
$$= e_1 1/(mP_c)(0,0,\ldots,0,d_c,-b_c,0,\ldots,0,0;0) + e_2(0,0,\ldots,0,0;1)$$

and

$$P_S = 1 - P\,,$$

where $P_c = \mathrm{Tr}C_c$. Carrying out the splitting by applying the projectors P and P_S to system (7) we obtain

$$\frac{\partial U_U}{\partial \tau} = 0 + P_1 N(U_U + U_S)\,,$$
$$\frac{\partial U_S}{\partial \tau} = P_S C U_S + P_S N(U_U + U_S) \tag{9}$$

because of $P_2 N(U_U + U_S) = 0$.

By the center manifold theory, as carried out in the Appendix, we get the following evolution equation for the amplitude of the linearly unstable mode e_1:

$$p_{,\tau} = \gamma(\Delta f')p + \beta p^3 + O(p^4 + |\Delta f' p^3| + (\Delta f')^2 p^2)\,, \tag{10}$$

with γ and β given by (A4). According to the center manifold approach the stability of the bifurcating solution is given by β. For $\beta < 0$ the spatially periodic solution is stable, for $\beta > 0$ it is unstable in the vicinity of the critical point. These cases are called supercritical and subcritical bifurcation, respectively.

Carrying out the same procedure for the system of equations (1) under neglect of the term $\delta w_{,xxt}$, which case is treated numerically in Ref. [28], we obtain an equation of the same form as Eq. (10). As can be seen from Eqs. (A4) and (A6) in the Appendix the parameters γ and β are only slightly varied. β has the same zero as before so that the qualitative behavior near the bifurcation point is the same as before. Theoretical investigations by means of perturbation theory were carried out by Elmer [37,38] and lead to similar results for the evolution equation of the amplitude.

$\Delta f'$ in Eq. (10) depends on system parameters, which can serve as bifurcation parameters. For this purpose we choose as reference point of the system the critical point so that $v = w = \chi = 0$ represents the bifurcation point with $F'(V_c, A_c) = f_c'$, $A_0 = A_c$, $r_0 = r_c$, $\kappa_0 = \kappa_c$, and $V_c = V_S(A_c, r_c, \kappa_c) = 0$. According to the experiments described later we consider the dependence of $\Delta f' = f'(V_c; A, r, \kappa) - f_c' = F'(V_S(A, r, \kappa), A) - F'(V_c, A_c)$ on the load resistor r, the applied voltage κ, and the width A of the nonlinear layer. Therefore we expand $\Delta f'$ in terms of differences $r - r_c$, $\kappa - \kappa_c$, and $A - A_c$ near the critical point (r_c, κ_c, A_c).

Expanding $F(V, A)$ at (V_c, A_c) up to the second order in V and A, and taking the partial derivative of this expansion with respect to V, we obtain the following equation for $\Delta f'$:

$$\Delta f' = f' - f_c' = \frac{\partial F}{\partial V}(V_S, A) - \frac{\partial F}{\partial V}(V_c, A_c)$$
$$= \frac{\partial^2 F}{\partial V^2}(V_c, A_c)(V_S - V_c) + \frac{1}{2}\frac{\partial^2 F}{\partial A^2}(V_c, A_c)(A - A_c)\,. \tag{11}$$

The relation between $(V_S - V_c)$ and $\Delta r, \Delta\kappa, \Delta A$ is obtained from the isocline system (2);

$$V_S - V_c = \frac{F(V, A) + \chi(A, r, \kappa)}{1 + r} - \frac{F(V_c, A_c)}{1 + r_c}\,. \tag{12}$$

Varying one of the parameters r, κ, A we have to choose the two other parameters as the critical values. Expanding $F(V, A)$ with $V = V(r, \kappa, A)$ at the critical value of the bifurcation parameter and taking into account only terms of the first order, we obtain, together with (11),

$$\Delta f' = \left[\frac{F_{,VV}(V_c, A_c)[F_{,A}(V_c, A_c) - \nu_A]}{1 + r_c} + \tfrac{1}{2}F_{,VA}(V_c, A_c)\right]\Delta A$$

for the variation of A,

$$\Delta f' = \frac{F_{,VV}(V_c, A_c)[(\partial F/\partial\kappa)(V_c, A_c) + 1]}{1 + r_c}\Delta\kappa$$

for the variation of κ, and

$$\Delta f' = \frac{F_{,VV}(V_c, A_c)[F_{,r}(V_c, A_c) + \nu_r - F(V_c, A_c)/(1 + r_c)]}{1 + r_c}\Delta r$$

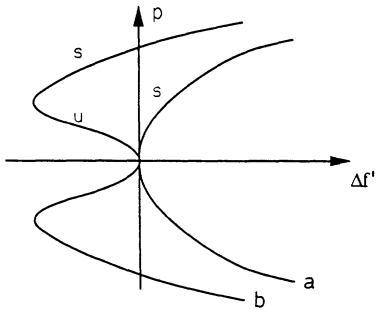

FIG. 4. Schematical presentation of the amplitude p of the critical mode as function of the bifurcation parameter $\Delta f'$ for (a) the supercritical and (b) the subcritical bifurcation; s denotes stable, u unstable branches of the amplitude curve.

for the variation of r.

From (10) we obtain the complete amplitude equation for the unstable mode with the wave number $2k_c$ dependent upon the three bifurcation parameters. Depending on the sign of β in Eq. (10) we obtain a supercritical or a subcritical bifurcation (see Fig. 4). β is a function of σ, so the parameters of an experiment can be chosen in a way that a supercritical or a subcritical bifurcation is obtained.

III. EXPERIMENTAL RESULTS

Figure 5 shows the experimental setup of the gas-discharge system consisting of two rectangular electrodes, one of which is of copper, while the other one is of n-type doped silicon monocrystal with a specific resistance of 0.5–0.9 kΩ cm. The semiconductor electrode has typical dimensions of $0.3\times10\times40$ mm^3 and has a thin aluminum layer as an Ohmic contact. The width of the gas-discharge gap can be varied in the range of 0.5–6 mm. The front end of the electrodes has dimensions of about 0.3×40 mm^2 and can be regarded as quasi-one-dimensional. The whole electrode system is covered by glass plates. A water cooling system serves to hold the arrangement on a fixed temperature during experiments. The experimental arrangement is in a vacuum recipient which contains He with a pressure of about 50–250 hPa.

The electrodes are connected with a high-voltage dc power supply by a shunt resistor R_S, which serves to limit the current through the gas-discharge system and to enable an approximately current-controlled operation of the discharge. Besides the quantities current and voltage we measure the light density distribution parallel to the discharge gap. For this purpose we observe the discharge slit with a vidicon camera. A special electronic arrangement serves to specify a video line from the positive column of the discharge slit. The video line signal, the amplitude of which is an appropriate measure for the light density distribution, is given on a digital storage oscilloscope.

The entire measurement arrangement can be seen in Fig. 6. The x-y recorder serves for the measurement of the $I(U_Y)$ characteristic. The video camera records the stationary spatial light density distribution and is connected with a digital oscilloscope.

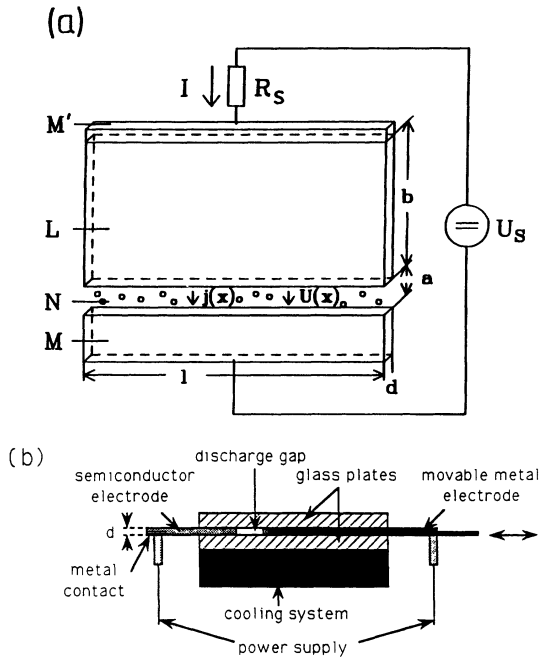

FIG. 5. (a) Schematical arrangement of the gas-discharge system according to the model in Fig. 1. U_S denotes the voltage supply, R_S the load resistance, M' the aluminum contact of the n-type or p-type doped silicon electrode L, N the gas gap, and M the copper electrode. (b) Cross section through the gas-discharge system showing the arrangement of the electrodes and the glass plates; the distance between the electrodes is 2–8 mm, the glass plates have a distance of 0.3 mm.

In the experiments the behavior of the stationary light intensity distribution transversal to the current flow in the discharge gap is observed under the influence of a variation of the applied voltage U_S, the load resistance R_S, or the width of the discharge gap. For an appropriate parameter range we observe two basic scenarios when varying these parameters. The first one is characterized by a spatially periodic pattern growing up continuously; in the other case, a discontinuous jump into an inhomogeneous distribution takes place. In the following we describe experiments concerning these two scenarios. The starting point for the experiments is a stable stationary conductive state, which is homogeneous in the direction parallel to the electrodes.

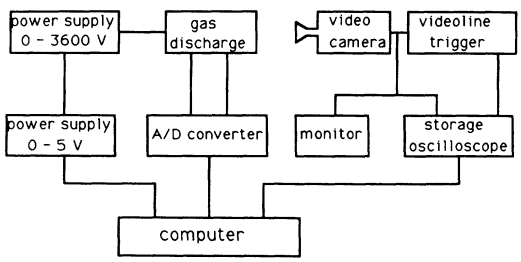

FIG. 6. Schematical setup for measuring the spatial distribution of the radiation density and the $I(U_N)$ characteristic.

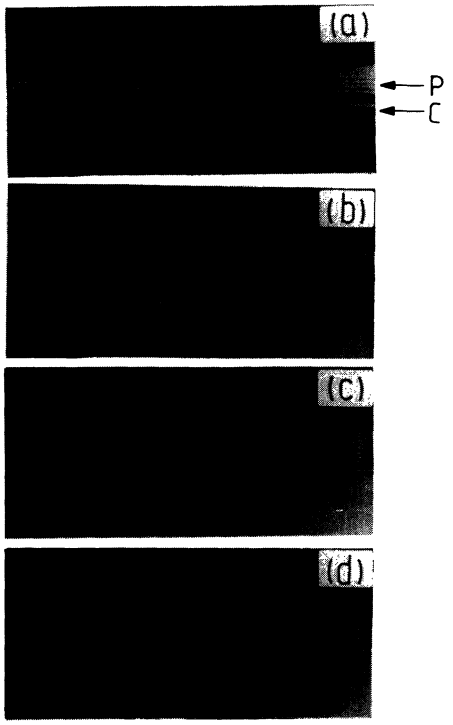

FIG. 7. Photographs of the discharge slit for decreasing applied voltage. The gas slit can be divided into the positive column (P) and the cathode layer (C). The bifurcation takes place in the positive column. Parameters: $R_S=25$ kΩ, $p=90$ hPa, $\rho=0.9$ kΩ cm, $a=4.5$ mm, $b=12$ mm, $d=0.3$ mm, $l=45$ mm. (a) $U_S=1500$ V, (b) $U_S=1020$ V, (c) $U_S=910$ V, (d) $U_S=800$ V.

Experiment No. 1

In Fig. 7(a) we see a discharge, which is homogeneous in the x direction and shows a spatial structure in the z direction consisting of different dark and bright regions, as there are the Aston and Faraday dark space, the negative glow, the positive column, etc. In the following investigations we roughly divide the discharge space into two parts, the positive column and the cathode region including all the dark and bright regions in front of the cathode. In the system described the cathode region has a width of about 0.5 mm.

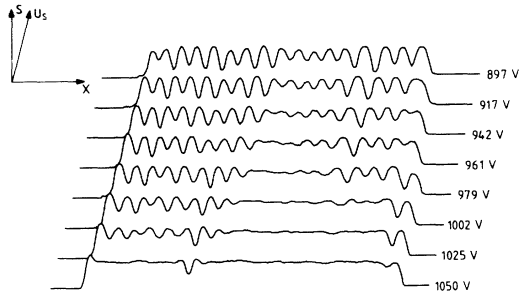

FIG. 8. Spatial distribution of the radiation density S for experiment No. 1 under variation of the applied voltage U_S. Parameters: $R_S=35.2$ kΩ, $p=120$ hPa, $\rho=0.53$ kΩ cm, $a=3$ mm, $b=12.5$ mm, $d=0.29$ mm, $l=34$ mm.

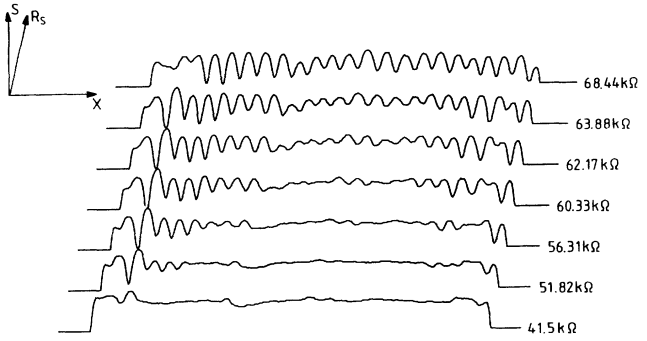

FIG. 9. Spatial distribution of the radiation density S for experiment No. 2 under variation of the load resistance R_S. Parameters: $U_S=1616$ V, $p=120$ hPa, $\rho=0.53$ kΩ cm, $l=38$ mm, $d=0.29$ mm, $b=12.5$ mm, $a=3.2$ mm.

In the first experiment the external supply voltage U_S is varied. In Figs. 7(a)–7(d) photographs of the discharge slit for different voltages are presented.

Figure 8 shows the spatial distribution of the radiation density for varying U_S. For large voltage ($U_S=1058$ V) we see a nearly homogeneous distribution with unavoidable small spatial inhomogeneities. When decreasing U_S a spatially periodic pattern with an intrinsic wave number increases continuously. Increasing the applied voltage, the structure would disappear in the same continuous way without hysteresis. The intrinsic wave number k_c normed on the diffusion constant d_W can be determined from the experimental results in Fig. 8 as $k_c=\pi n d_W^{1/2}/L$, where n is the number of half waves. For a voltage of 1025 V we could $n=28$ on a length of 28.2 mm. This leads to $k_c=17.1$.

Experiment No. 2

In this experiment the load resistance R_S is varied. Figure 9 shows the evolution of the light density distribution when increasing the load resistance. The parameters are chosen in a way that the transition is continuous and

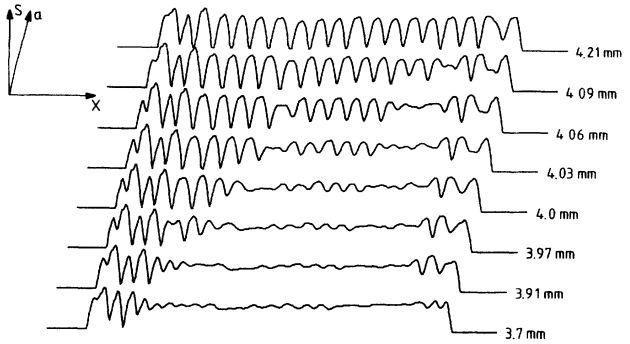

FIG. 10. Spatial distribution of the radiation density S for experiment No. 3 under variation of the width of the discharge slit. Parameters: $R_S=35.2$ kΩ, $U_S=1478$ V, $p=120$ hPa, $\rho=0.53$ kΩ cm, $l=38$ mm, $d=0.29$ mm, $b=12.5$ mm.

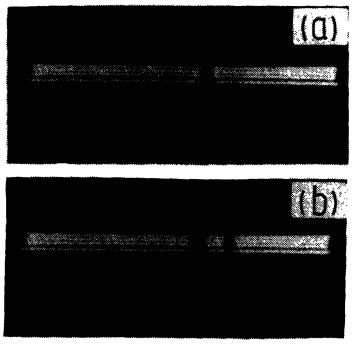

FIG. 11. Photographs of a subcritical bifurcation into a nonperiodic pattern. Parameters: $R_S=74.7$ kΩ, $p=244$ hPa, $\rho=0.9$ kΩ cm, $l=28$ mm, $d=0.22$ mm, $b=7.5$ mm, $a=1.5$ mm, (a) $U_S=1897$ V, (b) $U_S=1694$ V.

reversible without any hysteresis. We found $n=38$ for $L=31.3$ mm so that the half wave number is $k_c=20.9$.

Experiment No. 3

This experiment is concerned with the variation of the distance of the electrodes. When increasing the distance the typical distribution of an intrinsic wavelength occurs as to be seen in Fig. 10; the corresponding half wave number is $k_c=17.5$ with $n=30$, $L=29.6$ mm. For a further increase of the distance the system develops into a filamentary mode. This behavior is described in Ref. [26].

Experiment No. 4

Carrying out a similar experiment as in experiment No. 1, but choosing a small electrode distance and a high gas pressure, we observe a discontinuity jump into a spatially inhomogeneous nonperiodic pattern (Fig. 11).

IV. APPLICATION OF THE MODEL TO THE EXPERIMENTAL RESULTS— ADDITIONAL EXPERIMENTS

In order to apply the model to the experiments described above we have to define the linear and nonlinear regions within the z axis. Furthermore, we have to determine the parameters and the characteristic of the nonlinear layer. With physical reasons the qualitative behavior of the total current density must be the same as that of the partial current density of the model. Furthermore, for small deviations from the reference point we also get small quantitative differences. In the following we therefore replace the partial current density of the model by the total current density, i.e., $j=j_{\text{tot}}$.

From the experiments we see that the formation of periodic structure takes place in the positive column, while the cathode region is still homogeneously glowing. This is a motivation to check whether the positive column can serve as nonlinear layer in that it shows the required properties for a Turing instability rather than the whole discharge space including the cathode region.

The local characteristic $H(j,z_1,z_2)$ of a layer, which is the potential difference between z_1 and z_2 as function of j, is given by the integral over the electric field $E(j,z)$,

$$H(j,z_1,z_2)=\int_{z_1}^{z_2}E(j,z)dz\ .$$

In the following we describe experiments to determine this local characteristic for the positive column. To avoid structure formation in the x direction we use a small discharge element consisting of two copper electrodes, which have a front area of 0.3×1.0 mm^2. The discharge gap is covered by glass in all directions. By variation of the position z of one electrode (Fig. 12) we get different characteristics $H(j,0,z)$. If the electrode distance is very small (about 0.5 mm), there is no positive column and we get the $j(U_K)$ characteristic of the cathode region with $U_K=H(j,0,z_K)$ and z_K the extension of the cathode region.

In a first approximation we suppose that in the cathode region the electric field remains unchanged under variation of the distance of the electrodes. To determine the $j(U_P)$ characteristic of the positive column we form the difference between the $j(U_V)$ characteristic of the whole discharge and the $j(U_K)$ characteristic of the cathode region with

$$U_P=H(j,z_K,z_K+z_P)\ ,$$

$$U_V=H(j,0,z_K+z_P),$$

$$U_K=H(j,0,z_K)\ ,$$

and z_K and z_P the extension of the cathode region and the positive column, respectively (see Fig. 12).

From the theoretical investigations in Sec. II we know that the Turing instability occurs for a critical ratio of the slopes of the load line and the nonlinear function at the operating point. Especially the bifurcation takes

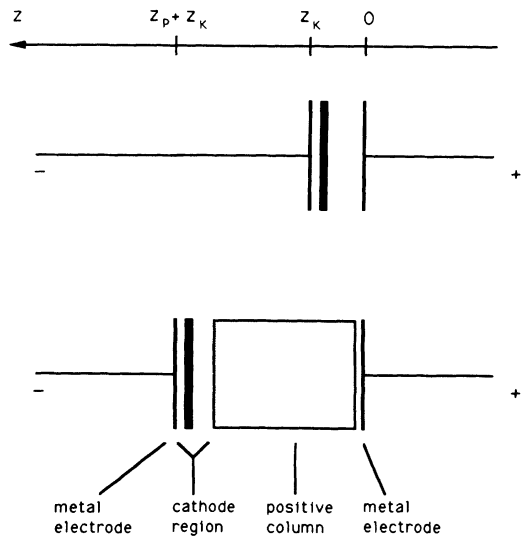

FIG. 12. Schematical spatial distribution of the cathode region and the positive column for various electrode distances; the positive metal electrode is placed at $z=0$, z_K and z_P denote the extension of the cathode region and the positive column, respectively.

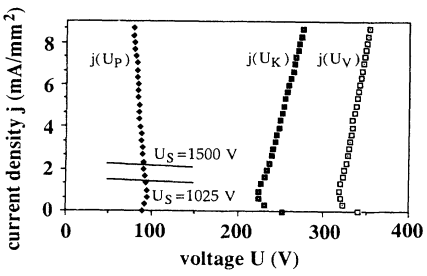

FIG. 13. $j(U_p)$ characteristic of the positive column, $j(U_K)$ characteristic of the cathode region, and $j(U_V)$ characteristic of the whole discharge. The load line refers to the $j(U_P)$ characteristic and is shifted in parallel with varying voltage U_S. Parameters are the same as in Fig. 8.

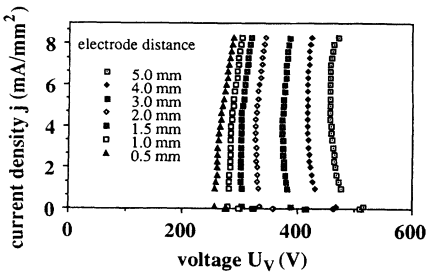

FIG. 15. $j(U_V)$ characteristics of the whole discharge space for various distances of the electrodes. For the distance of 0.5 mm the positive column disappears and the characteristic of the cathode region is obtained. Parameters are the same as in Fig. 10.

place in a region where the nonlinear characteristic of the model has a negative differential slope. Experimentally bifurcations from the homogeneous into a periodic state have been realized with the voltage U_S, the resistance R_S, and the electrode distance as bifurcation parameters in the gas-discharge system consisting of a metal and a semiconductor electrode. To identify the nonlinear layer we have a look at the slopes of the three characteristics in the respective operation point, which is defined by the current density at which the instability occurs. Figures 13 and 14 show the three characteristics of the experiments Nos. 1 and 2, which refer to the bifurcations by varying the applied voltage U_S or the load resistance R_S (cf. Figs. 8 and 9). The dashed lines indicate the current at which the bifurcation sets in. The load lines (solid) refer to the $j(U_P)$ characteristic. The slopes of these load lines are determined by the load resistance R_S, the resistance of the semiconductor electrode $\rho b/(ld)$, and the resistance of the cathode region. The latter can be estimated by the $j(U_K)$ characteristic which is nearly linear in the vicinity of the bifurcation point.

The same type of bifurcation is observed when increasing the electrode distance, i.e., increasing the width of the positive column (cf. Fig. 10). Figure 15 shows the $j(U_V)$ characteristics of the homogeneous discharge for various distances, Fig. 16 the respective characteristics of the positive column. We see that for fixed load line obtained as described above the operating point in the $j(U_P)$ characteristic is shifted into the critical region by increasing the distance of the electrodes.

In all cases we observe that the slope of the $j(U_K)$ characteristic in the bifurcation point is positive, that of the $j(U_P)$ characteristic negative, whereas the slope of the global $j(U_V)$ characteristic can be either positive or negative. According to these considerations we conclude that the bifurcation into a spatially periodic state takes place in the positive column. Therefore it is plausible to locate the nonlinear layer in the positive column.

While the examples Nos. 1–3 can be explained by a supercritical bifurcation of the model, the experiment No. 4 is related to the subcritical bifurcation, which corresponds to the case $\beta>0$ in Sec. II. The case that a periodic structure appears discontinuously was not observed up to now; instead we obtain a transition to a nonperiodic structure. One reason may be that our samples have too many intrinsic inhomogeneities. By the above examples we can state that the predictions of the two-layer model and the experimental results are qualitatively in good agreement concerning the formation of spatially periodic patterns. We may conclude that the characteristic of the positive column can be approximated in the vicinity of the critical point by a cubic polynomial, the parameters of which match the type of the corresponding bifurcation.

As the first quantitative advance we investigate whether the insertion of the experimentally observed wave

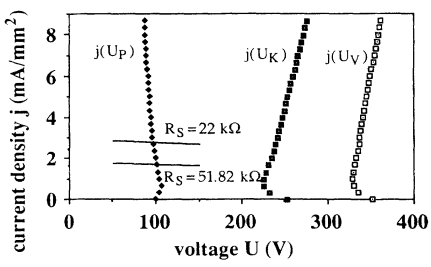

FIG. 14. $j(U_P)$ characteristic of the positive column, $j(U_K)$ characteristic of the cathode region, and $j(U_V)$ characteristic of the whole discharge. The load line refers to the $j(U_P)$ characteristic and is tilted with varying resistance R_S. Parameters are the same as in Fig. 9.

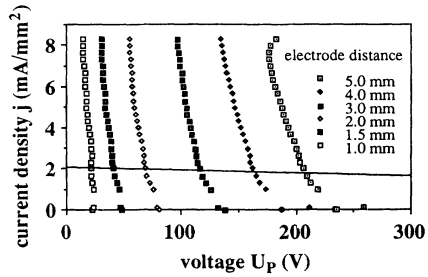

FIG. 16. $j(U_P)$ characteristics of the positive column obtained from the $j(U_V)$ characteristics of Fig. 15 by subtracting the $j(U_K)$ characteristic of the cathode region. The operation point on the $j(U_P)$ characteristic is shifted into the critical region when increasing the electrode distance.

TABLE I. Ampipolar diffusion constant D_0 obtained from the experiments Nos. 1–3 by measuring the length a of the discharge gap and the wave number k_c of the periodic structure, and by determining the current density j_b and the distributed inductivity ℓ at the bifurcation point.

No.	a (mm)	j_b (mA/mm^2)	ℓ(V s m^2/A)	k_c	D_0 (cm^2/s)
1	3.0	1.5	16	17.1	15
2	3.2	2.0	15	20.9	7
3	3.7	2.4	14	17.5	15

number into the model leads to a reasonable value for D_0. Eliminating σ from Eqs. (1d) and (6a) and solving to D_0 we obtain

$$D_0=\frac{5b^3\rho}{26\ell(k_c^2+1)^2} .$$

The specific resistance of the semiconductor electrode is $\rho=0.53$ kΩ cm and the thickness of the electrode is $b=1.25$ cm. The time τ, which passes until the current density reaches its stationary value after an increase of the voltage U between the two metal electrodes, was estimated by means of a pulsed discharge in the arrangement for the measurement of the local characteristic. ℓ is given by the product of the time τ and the slope of the $U(j)$ characteristic $\ell\approx\tau\partial U/\partial j\approx 8\times 10^{-9}$ V s m^2/A.

For the experiments in Sec. III we get Table I. The diffusion constants D^- and D^+ of the electrons and the positive He ions, respectively, are estimated with regard to the pressure corresponding to the experiment and the temperature 293 K according to Ref. [39]. We obtain D^+ in the range of 1.1–4.5 cm^2/s and D^- in the range of 226–452 cm^2/s. The experimentally determined ambipolar diffusion constant D_0 is in a reasonable range between the diffusion constants of the electrons and the positive He ions. This is a good confirmation for the assumption of ambipolar drift effects used in the derivation of Eqs. (1).

V. CONCLUSIONS

For a dc gas-discharge system consisting of a copper and a semiconductor electrode covered by glass plates we have shown some experiments concerning the evolution of patterns lateral to the current flow. When varying appropriate parameters the formation of spatially periodic structures emerging from a homogeneously glowing state takes place. These periodic structures are predicted by a two-layer model, the physical behavior of which can be described by a two-component reaction-diffusion system. We have shown from bifurcation analysis that a stationary homogeneous solution of the equation system is unstable with respect to a perturbation of a special critical wavelength at a critical slope of the nonlinearity $f(v)$ corresponding to the $j(U)$ characteristic of the nonlinear layer in the gas-discharge system. This critical point can be attained in several ways by variation of system parameters, which correspond to the experimentally varied quantities.

To explain the experimentally observed patterns by means of the model we had to identify the linear and the nonlinear layers of the model in the gas-discharge system. For this purpose the $I(U_V)$ characteristic of the whole discharge space and the $I(U_P)$ characteristic of the positive column were measured. From these experiments the nonlinear layer should be the positive column of the discharge. The experimental results are qualitatively in good agreement with the predictions of the model.

For a first quantitative approach the experimentally observed intrinsic wave number, which is coupled with the diffusion constant of the model, was used to estimate the ambipolar diffusion constant of the gas in the experimental arrangement. The result obtained is a reasonable value. This is a further confirmation for the application of the model to the gas-discharge system.

ACKNOWLEDGMENTS

The authors would like to thank N. Reese for his support in doing calculations. We gratefully acknowledge the support of the "Stiftung Volkswagenwerk."

APPENDIX

According to the double eigenvalue zero the system (9) has a two-dimensional center manifold, which is approximated by the ansatz

$$U_S(U_U,\Delta f')=U_S(p,\Delta f')=\Phi(p,\Delta f')+\vartheta .$$

According to Ref. [37] the error term ϑ of this approximation is of the same order as the functional M, which is defined by

$$M(\Phi)=(\partial\Phi/\partial p)P_1N(U_u+\Phi)-P_SC\Phi-P_SN(U_u+\Phi) , \tag{A1}$$

with $N=(N_{v0},0,\ldots,N_{vn},0,\ldots;0)$ and the property $M(U_S)=0$. Considering terms up to the third order we get for N_{vn}

$$N_{vn}=\langle\varphi_n|(\Delta f')v+(1/2!)f^{(2)}(0)v^2 +(1/3!)f^{(3)}(0)v^3+\mu(\nabla v)(\nabla w)\rangle. \tag{A2}$$

For an ansatz $\Phi(p,\Delta f')=Ap^2+B(\Delta f')p$ we can show that $M(\Phi)$ is of third order in p and $\Delta f'$ for appropriately chosen A and B, i.e., we can solve $M(U_S)=0$ up to third order in p and $\Delta f'$.

From Eq. (A1) together with Eq. (A2) we obtain the following equation to determine the vectors A and B:

$$P_S C[Ap^2+B(\Delta f')p] = -P_S N(U_c+U_S)$$
$$= -p^2(g_0,0,0,0,\ldots,0,0,g_{2c},0,0,0,\ldots,0,0;0)^T$$
$$-(\Delta f')p(0,0,\ldots,0,0,\rho_c,\rho_c^*,0,0,\ldots,0,0;0)^T+O(|p^3|+|\Delta f'|p^2+(\Delta f')^2|p|)\ ,$$

with $g_0=m^2L^{-1/2}(\frac{1}{2}f_c^{(2)}+\mu k_c^2 a_c)$, $g_{2c}=m^2(2L)^{-1/2}(\frac{1}{2}f_c^{(2)}-\mu k_c^2 a_c)$, $\rho_c=ma_c/P_c$, and $\rho_c^*=ma_c d_c/(b_c P_c)$, where $f_c^{(2)}=f^{(2)}(0;A_c,r_c,\kappa_c)$. The solution is

$$A=(A_{v0},A_{w0},0,0,\ldots,0,0,A_{v2c},A_{w2c},0,0,\ldots,0,0;0)^T\ ,$$
$$B=(0,0,\ldots,0,0,B_{vc},B_{wc},0,0,\ldots,0,0;0)^T\ ,$$

with

$$A_{v0}=-g_0 d_0/|C_0|,\quad A_{w0}=g_0 c_0/|C_0|\ ,$$
$$A_{v2c}=-g_{2c}d_{2c}/|C_{2c}|,\quad A_{w2c}=g_{2c}c_{2c}/|C_{2c}|\ , \tag{A3}$$
$$B_{vc}=-\rho_c/P_c,\quad B_{wc}=-\rho_c^*/P_c\ ,$$

where $|C_n|=\det C_n$. Inserting this approximation for U_S we obtain from the first equation of (9)

$$p_{,\tau}e_1=P_1N=e_1[\gamma(\Delta f')p+\beta p^3]$$
$$+O(p^4|\Delta f' p^3|+(\Delta f')^2p^2)\ ,$$

with

$$\gamma(\Delta f')=\frac{d_c}{P_c}\Delta f'-\frac{a_c d_c}{P_c^3}(\Delta f')^2$$

and

$$\beta=\frac{d_c}{L^{1/2}P_c}\left[-\left[\frac{g_0 d_0}{|C_0|}+\frac{g_{2c}d_{2c}}{2^{1/2}|C_{2c}|}\right]f_c^{(2)}\right.$$
$$\left.+\frac{m^2}{4L^{1/2}}f_c^{(3)}+\frac{2^{1/2}g_{2c}k_c^2\mu(a_c d_{2c}-c_{2c})}{|C_{2c}|}\right]\ .$$

With k_c and f_c' from (6) we can write β and γ in terms of the system parameters and obtain

$$\beta=\frac{\Gamma+\Gamma_m+\Gamma_r+\Gamma_{mr}}{4L(1+\sigma)(1-\delta\sigma^{1/2})}\ , \tag{A4a}$$

with

$$\Gamma=f_c^{(3)}+(f_c^{(2)})^2\frac{15\sigma^{1/2}+4}{9\sigma^{1/2}(\sigma^{1/2}-1)^2}\ ,$$
$$\Gamma_r=\frac{-2r(f_c^{(2)})^2}{(\sigma^{1/2}-1)^2[(\sigma^{1/2}-1)^2+r]}\ ,$$
$$\Gamma_m=\frac{-4\mu^2}{9}+\frac{38f_c^{(2)}\mu}{9(\sigma^{1/2}-1)}\ ,$$
$$\Gamma_{mr}=\frac{4\mu r}{(1-\sigma^{1/2})[(\sigma^{1/2}-1)^2+r]}\ ,$$

and

$$\gamma(\Delta f')=\frac{\Delta f'}{1-\sigma^{1/2}\delta}-\frac{\sigma^{1/2}\delta^2(\Delta f')^2}{(1-\sigma^{1/2}\delta)^3}\ . \tag{A4b}$$

In this way we get the evolution equation for the amplitude of the linearly unstable mode e_1,

$$p_{,\tau}=\gamma(\Delta f')p+\beta p^3+O(p^4+|\Delta f' p^3|+(\Delta f')^2p^2)\ , \tag{A5}$$

with γ and β given by (A4a) and (A4b), respectively.

Carrying out the same procedure for the system of equations (1) and neglecting the term $\delta w_{,xxt}$, we obtain an equation of the same form as Eq. (A5). The parameters γ and β are slightly varied into

$$\gamma(\Delta f')=\frac{\Delta f'}{1-\delta\sigma}-\frac{\sigma^{3/2}\delta^2(\Delta f')^2}{(1-\sigma\delta)^3}\ ,$$
$$\beta=\frac{\Gamma+\Gamma_m+\Gamma_r+\Gamma_{mr}}{4L(1+\sigma)(1-\delta\sigma)}\ . \tag{A6}$$

*Present address: Department of Electrical and Computer Engineering, University of Colorado at Boulder, Boulder, CO 80309.

[1] B. P. Belousov (unpublished); A. M. Zhabotinsky and A. N. Zaikin, J. Theor. Biol. **40**, 45 (1973).
[2] L. A. Lugiato, C. Oldano, and L. M. Narducci, J. Opt. Soc. Am. B **5**, 880 (1988).
[3] *Nonlinear Phenomena in Physics,* edited by F. Claro (Springer, Berlin, 1984).
[4] A. Gierer and M. Meinhardt, Lect. Math. Life Sci. **7**, 163 (1974).
[5] H. Haken, *Synergetics—An Introduction* (Springer, Berlin, 1978).
[6] G. Nicolis and I. Prigogine, *Self-Organization in Non-Equilibrium Systems* (Wiley, New York, 1977).
[7] F. J. Elmer, Physica D **30** 321 (1988).
[8] M. Büttiker and H. Thomas, Phys. Rev. A **24**, 2635 (1981).
[9] V. L. Bonc-Bruevic, I. P. Zvyagin, and A. G. Mirnov, *Domain Electrical Instabilities in Semiconductors, Studies in Soviet Sciences* (Consult Bureau, New York, 1975).
[10] A. M. Barnett, in *Current Filament Formation in Semiconductor and Semimetals 6, Injection Phenomena,* edited by R. K. Willardson and R. C. Beer (Academic, New York, 1970).
[11] H. Baumann, R. Symanczyk, C. Radehaus, H.-G. Purwins, and D. Jäger, Phys. Lett. A **123**, 421 (1987).

[12] H. Baumann, Ph.D. thesis, University of Münster, 1988.
[13] D. Jäger, H. Baumann, and R. Symanczyk, Phys. Lett. A **117**, 141 (1986).
[14] K. Kardell, C. Radehaus, R. Dohmen, and H.-G. Purwins, J. Appl. Phys. **64**, 6336 (1988).
[15] E. Schöll, *Nonequilibrium Phase Transitions in Semiconductors* (Springer, Berlin, 1987).
[16] B. S. Kerner and V. F. Sinkevich, Zh. Eksp, Teor. Fiz. **83**, 359 (2982) [Sov. Phys.—JETP **56**, 196 (1982)].
[17] B. S. Kerner and V. V. Osipov, Zh. Eksp. Teor. Fiz **79**, 2218 (1980) [Sov. Phys.—JETP **52**, 1122 (1980)].
[18] I. Grabec, Phys. Fluids **17**, 1834 (1974).
[19] K. Ohe, and K. Tsunoda, Contrib. Plasma Phys. **27**, 171 (1987).
[20] F. C. van den Heuvel, Philip Tech. Rev. **44**, 89 (1988).
[21] N. A. Kapzow, *Elektrische Vorgänge in Gasen und im Vakuum* (Deutscher Verlag der Wissenschaften, Berlin, 1955).
[22] D. G. Boyers and W. A. Tiller, J. Appl. Phys. **44**, 3102 (1973).
[23] D. G. Boyers and W. A. Tiller, Appl. Phys. Lett. **41**, 28 (1982).
[24] Yu. A. Astrov, and L. M. Portsel, Zh. Tekh. Fiz. **51**, 2502 (1981) [Sov. Phys.—Tech. Phys. **26**, 1480 (1981)].
[25] K. G. Müller, Phys. Rev. A **37**, 4836 (1988).
[26] C. Radehaus, T. Dirksmeyer, H. Willebrand, and H.-G. Purwins, Phys. Lett. A **125**, 92 (1987).
[27] C. Radehaus, K. Kardell, H. Baumann, D. Jäger, and H.-G. Purwins, Z. Phys. B **65**, 515 (1987).
[28] C. Radehaus, R. Dohmen, H. Willebrand, and F.-J. Niedernostheide, Phys. Rev. A **42**, 7426 (1990).
[29] C. Radehaus, Ph.D. thesis, University of Münster, 1987.
[30] H.-G. Purwins, C. Radehaus, and J. Berkemeier, Z. Naturforsch. A **43**, 17 (1988).
[31] H.-G. Purwins and C. Radehaus, in *Neural and Synergetic Computer,* edited by H. Haken, Springer Series in Synergetics Vol. 42 (Springer, Berlin, 1988).
[32] H.-G. Purwins, G. Klempt, and J. Berkemeier, Festkörperprobleme **27**, 27 (1987).
[33] J. Berkemeier, T. Dirksmeyer, G. Klempt, and H.-G. Purwins, Z. Phys. B **65**, 255 (1986).
[34] T. Dirksmeyer, R. Schmeling, J. Berkemeier, and H.-G. Purwins, in *Patterns, Defects and Materials Instabilities,* Vol. 183 of *NATO Advanced Study Institute, Series B: Physics,* edited by D. Walgraef and N. M. Ghoniem (Kluwer Academic, Dordrecht, 1990).
[35] T. Dirksmeyer, Ph.D. thesis, University of Münster, 1990.
[36] A. M. Turing, Philos. Trans. R. Soc. London Ser. B **237**, 37 (1952).
[37] J. Carr, *Applications of Centre Manifold Theory* (Springer, New York, 1981).
[38] F. J. Elmer (private communication).
[39] B. Gänger, *Der elektrische Durchschlag von Gasen* (Springer, Berlin, 1953).

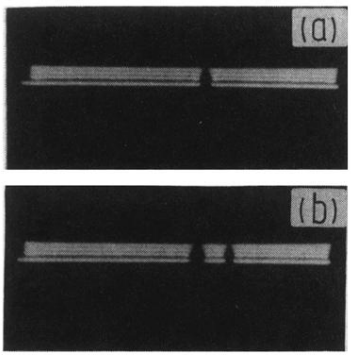

FIG. 11. Photographs of a subcritical bifurcation into a non-periodic pattern. Parameters: $R_S = 74.7$ kΩ, $p = 244$ hPa, $\rho = 0.9$ kΩ cm, $l = 28$ mm, $d = 0.22$ mm, $b = 7.5$ mm, $a = 1.5$ mm, (a) $U_S = 1897$ V, (b) $U_S = 1694$ V.

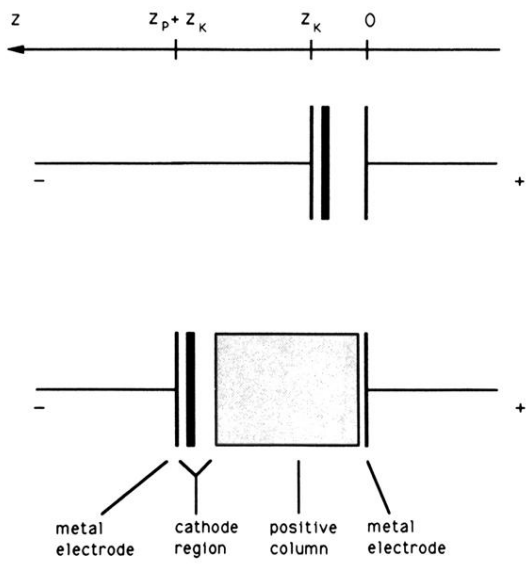

FIG. 12. Schematical spatial distribution of the cathode region and the positive column for various electrode distances; the positive metal electrode is placed at $z=0$, z_K and z_P denote the extension of the cathode region and the positive column, respectively.

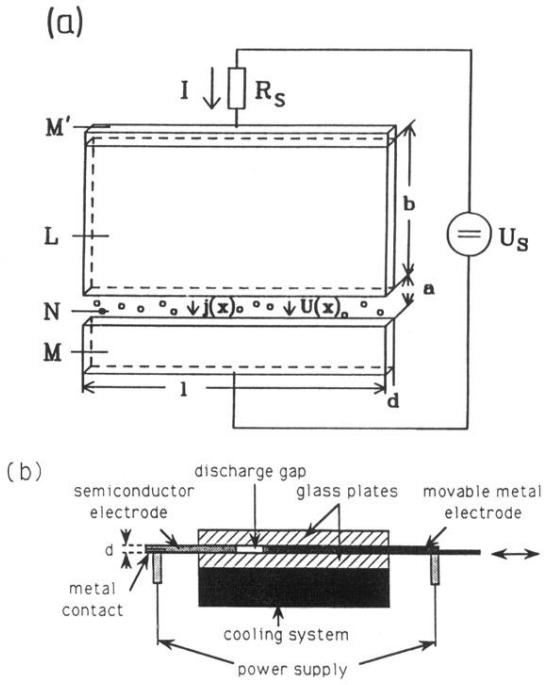

FIG. 5. (a) Schematical arrangement of the gas-discharge system according to the model in Fig. 1. U_S denotes the voltage supply, R_S the load resistance, M' the aluminum contact of the n-type or p-type doped silicon electrode L, N the gas gap, and M the copper electrode. (b) Cross section through the gas-discharge system showing the arrangement of the electrodes and the glass plates; the distance between the electrodes is 2–8 mm, the glass plates have a distance of 0.3 mm.

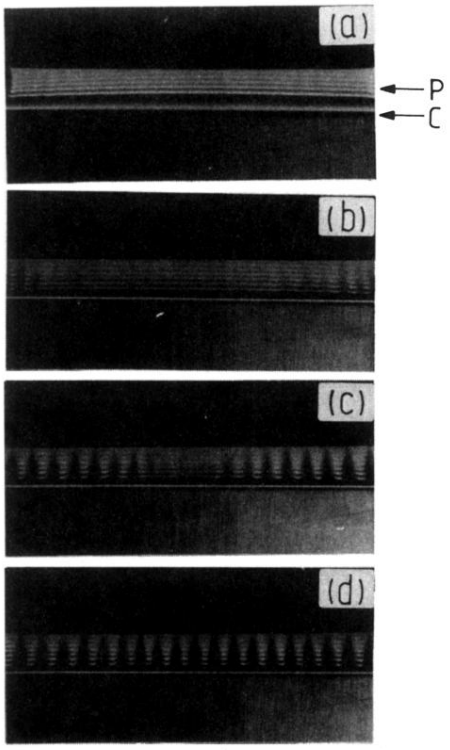

FIG. 7. Photographs of the discharge slit for decreasing applied voltage. The gas slit can be divided into the positive column (P) and the cathode layer (C). The bifurcation takes place in the positive column. Parameters: $R_S = 25$ kΩ, $p = 90$ hPa, $\rho = 0.9$ kΩ cm, $a = 4.5$ mm, $b = 12$ mm, $d = 0.3$ mm, $1 = 45$ mm. (a) $U_S = 1500$ V, (b) $U_S = 1020$ V, (c) $U_S = 910$ V, (d) $U_S = 800$ V.